Effects of temperature and hydrostatic pressure on the magnetoelasticity of a commensurate spin-density-wave antiferromagnetic Cr–3.5 at. % Al alloy single crystal

H. L. Alberts and P. Smit
Department of Physics, Rand Afrikaans University, P.O. Box 524, Auckland Park 2006, Johannesburg, South Africa
(Received 20 January 1995)

Measurements are reported of the temperature and hydrostatic-pressure dependences of the elastic constants and thermal expansion of a Cr–3.5 at. % Al alloy single crystal through the Néel transition. The magnetic contributions to the volume strain and bulk modulus have been found to fit the equation $a+bT^2+cT^4$, predicted by theory, rather well up to temperatures close to the Néel temperature (T_N). The pressure derivatives of the elastic constants at different constant temperatures are used to calculate the acoustic-mode Grüneisen parameters as a function of temperature through the Néel point. The mean long-wavelength acoustic Grüneisen parameter, $\overline{\gamma}^{el} \approx -5$, is negative in the commensurate spin-density-wave phase ($T < T_N$), it increases sharply to a positive value of $\overline{\gamma}^{el} \approx +35$ just above T_N and then decreases to a value $\overline{\gamma}^{el} \approx +2$ at temperatures well into the paramagnetic phase. The spin density wave couples mainly with the longitudinal-mode acoustic phonons in the long-wavelength limit. Shear-mode anharmonicity is only weakly affected by the Néel transition.

I. INTRODUCTION

The antiferromagnetic ordering in Cr and its dilute alloys is associated with a spin-density-wave (SDW) state.[1] The SDW is formed by condensation of electron-hole pairs from electrons in the electron sheet of the Fermi surface and holes on the hole sheet. In pure Cr the wave vector of the SDW is incommensurate (I) with the lattice parameter, giving rise to an ISDW state. When Cr is alloyed with an element, like for instance V, to lower the electron concentration, the SDW state remains incommensurate up to the concentration of about 4 at. % V where antiferromagnetism disappears.[1] On the other hand, when Cr is alloyed with a metal like Mn to increase the electron concentration, the SDW eventually becomes commensurate (C) with the lattice and a CSDW state is formed.[1] The magnetic phase diagrams of many dilute Cr-alloy systems are complex[1] in that they contain a triple point on the phase diagram where the three phases ISDW, CSDW, and paramagnetic (P) coexist. Examples are Cr-Ru, Cr-Re, Cr-Mn, etc.[1] In these systems a transformation ISDW→CSDW is observed with increasing temperature or applied pressure.

The SDW gives[1] rise to large magnetic contributions to the elastic constants of Cr and its dilute alloys. This is indicative of strong magnetoelastic coupling. Magnetoelastic effects are exceptionally large in the Cr-Al system, amounting[2] to a magnetic contribution of about 50% to the bulk modulus of a Cr–2.2 at. % Al alloy at low temperatures. It also gives rise to an anomaly in the elastic constants at the ISDW-CSDW phase transition temperature.[1] The effects of temperature and alloying on the magnetoelastic properties of Cr and its dilute alloys have been studied extensively in the past.[1] The effects of applied pressure on these properties were however studied in detail only recently.[3] These recent studies reported on a comprehensive experimental study of the effects of applied pressure on the elastic properties at the ISDW-CSDW phase transition of a Cr–0.3 at. % Ru alloy. The acoustic-mode Grüneisen parameters in both the ISDW and CSDW phases were obtained for this alloy. The longitudinal-mode Grüneisen parameter is large and negative in both phases, being much larger in magnitude for the CSDW phase, while the shear-mode Grüneisen parameters are small and positive in both phases. It was concluded that the strong magnetoelastic coupling at the ISDW-CSDW transition of Cr–0.3 at. % Ru takes place mainly through volume strain but there are also contributions from shear strain.

Studies on the effects of applied pressure on the magnetoelasticity of Cr and Cr alloys near the Néel point (T_N) are scarce. The case of pure Cr which shows an ISDW-P transition at T_N was studied by Katahara *et al.*[4] but similar studies do, however, not exist for alloys showing a CSDW-P transition at T_N.

In the present work a detailed study of the effects of hydrostatic pressure on the elastic constants through the CSDW-P transition of a Cr–3.5 at. % Al single crystal is reported. The Cr-Al system was chosen for its large magnetoelastic effects[5,6] and the concentration of 3.5 at. % Al gives a CSDW-P transition at T_N with no ISDW-CSDW transition at lower temperatures.[1] The Néel point for this concentration at atmospheric pressure is furthermore situated close to room temperature, making the alloy ideally suited for high-pressure ultrasonic measurements. The results are used to obtain the acoustic-mode Grüneisen parameters which give information on the acoustic-phonon interaction with the SDW as well as information on the role of volume and shear strains in the CSDW-P transition.

II. EXPERIMENTAL METHODS

The Cr–3.5 at. % Al crystal was grown from 99.996% pure iochrome and 99.99% Al by a floating-zone technique using RF heating in a pure argon atmosphere. A bar of the alloy, roughly cylindrical in form, of length about 10 cm and diameter between 7 and 10 mm was first

0163-1829/95/51(21)/15146(10)/$06.00

prepared by RF melting in a horizontal cold crucible. This bar was then grown to a single crystal of length about 5 cm and diameter about 6 mm by the floating-zone technique with the bar in a vertical position. Electron microprobe analyses at different positions on the crystal show that it is homogeneous to within 7% of the quoted concentration and that the actual concentration of 3.37 at. % Al differs on the average by about 4% from the above quoted nominal concentration. The crystal was prepared with flat (100) and (110) faces for ultrasonic measurements by spark planing. The distance between the (110) faces is about 7.5 mm and that between the (100) faces about 6.6 mm. Standard phase comparison[7] or pulse-echo overlap[8] ultrasonic techniques were used to measure the temperature dependence of longitudinal and shear-wave velocities for wave propagation along [100] or [110]. The phase comparison method was found to be particularly useful for longitudinal-wave velocity measurements as a function of temperature for which the velocity change at T_N is relatively large. The small changes in velocity with applied pressure were measured using the pulse-echo overlap technique. The sensitivity of this technique is 1 part in 10^5, while that of the phase comparison method is between 1 part in 10^3 and 1 part in 10^4. The error in the absolute values of the sound velocities is about 0.5%. 10 MHz X-cut or Y-cut quartz transducers were used to generate, respectively, longitudinal and shear waves. The transducers were bonded to the crystal with epoxy resin. Velocity data were corrected for transducer diffraction effects by using methods developed by Kittinger.[9] Hydrostatic pressure in the pressure range 0 to 0.16 GPa was generated by a high-pressure gas system using nitrogen gas as the pressure medium. Pressure runs were done at constant fixed temperatures in the range 246 to 374 K. The temperature was kept constant to within 0.2 K or better during pressure runs.

Thermal expansion of the crystal along [100] was also measured as a function of temperature using strain gauge techniques. These measurements were made relative to Cr–5 at. % V, which remains paramagnetic at all temperatures and serves to simulate[5] the nonmagnetic component of the Cr–3.5 at. % Al alloy, i.e., $(\Delta L/L)_{\text{meas}}=(\Delta L/L)_{\text{Cr-V}}-(\Delta L/L)_{\text{Cr-Al}}$. The error in the absolute values of $\Delta L/L$ is about 5%, while changes of 3×10^{-7} with temperature could be detected.

Ultrasonic and thermal-expansion measurements at atmospheric pressure were done in the temperature range 77–450 K by heating the sample slowly at a rate of about 0.6 K per minute for the ultrasonic experiments and at about 0.06 K per minute for the thermal-expansion measurements. The latter measurements were recorded at 0.05 K intervals. Heating and cooling runs during the thermal-expansion measurements show no hysteresis effects.

III. EXPERIMENTAL RESULTS FOR THE TEMPERATURE DEPENDENCE OF THE ELASTIC CONSTANTS AND THERMAL EXPANSION

Figure 1 shows the temperature dependence of the adiabatic elastic constants c_{11}, $c_L=\frac{1}{2}(c_{11}+c_{12}+2c_{44})$, $c'=\frac{1}{2}(c_{11}-c_{12})$, c_{44} and $B=\frac{1}{3}(c_{11}+2c_{12})$ at atmospheric pressure. The magnetovolume is directly given by $\Delta\omega=3(\Delta L/L)_{\text{meas}}$. It is negative and its absolute value is shown for [100] measurements in Fig. 2(a). Thermal-expansion effects are too small to affect the elastic constant data significantly, being within the experimental error.

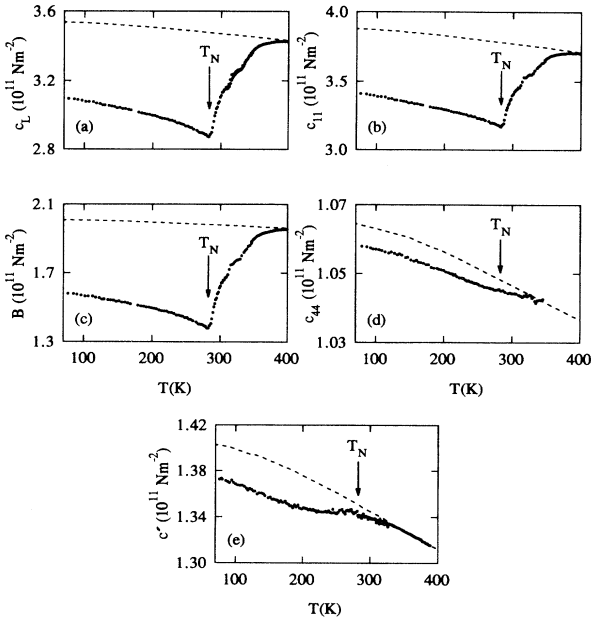

FIG. 1. Elastic constants of Cr–3.5 at. % Al as a function of temperature. (a) $c_L=\frac{1}{2}(c_{11}+c_{12}+2c_{44})$, (b) c_{11}, (c) $B=\frac{1}{3}(c_{11}+2c_{12})$, (d) c_{44}, and (e) $c'=\frac{1}{2}(c_{11}-c_{12})$. The broken curves are the expected nonmagnetic behavior determined from results of Cr–5 at. % V. The dashes in these broken curves connect the experimental points for Cr–5 at. % V as obtained from Ref. 10.

The temperature dependence of the elastic constants of a Cr–5 at. % V single crystal,[10] which remains paramagnetic at all temperatures, was used as a reference for the expected temperature dependence of the nonmagnetic behavior of c_{11}, c_L, c', c_{44}, and B. This nonmagnetic behavior is also shown in Fig. 1. The curves for Cr–5 at. % V (Ref. 10) of the corresponding elastic constants in Fig. 1 were shifted slightly up or down to coincide as closely as possible with the high-temperature measurements of the Cr–3.5 at. % Al crystal. The results of Roberts, White, and Fawcett[11] for the coefficient of thermal expansion ($\alpha_{Cr_{95}V_5}$) of Cr–5 at. % V were used to calculate the coefficient of thermal expansion $\alpha_{\text{Cr-Al}}$ of the Cr–3.5 at. % Al crystal from $(\Delta L/L)_{\text{meas}}$. The results are shown in Fig. 2(b) together with $\alpha_{Cr_{95}V_5}$ which simulates the nonmagnetic component of $\alpha_{\text{Cr-Al}}$. $\alpha_{\text{Cr-Al}}$ is shown as a smooth curve in Fig. 2(b). The scattering of the calculated $\alpha_{\text{Cr-Al}}$ around this curve is within $\pm0.1\times10^{-6}$ K^{-1}.

The c_{11}-T and B-T curves in Fig. 1 show a minimum at (282.5±0.6) K which corresponds with the temperature of (280±2) K at which the minimum is observed in the

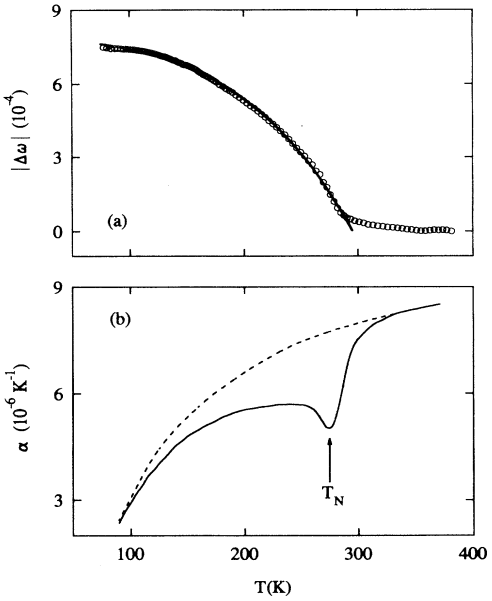

FIG. 2. The temperature dependence of (a) the absolute value of the magnetovolume $|\Delta\omega|$ and (b) the coefficient of thermal expansion α of Cr–3.5 at. % Al measured along [100]. The broken curve in (b) represents α for Cr–5 at. % V obtained from Ref. 11 and represents the expected nonmagnetic behavior of α for the Cr–3.5 at. % Al crystal. The solid curve in (a) represents the best fit to the equation $\Delta\omega = a_2 + b_2 t^2 + c_2 t^4$, where $t = T/T_N$ and the coefficients a_2, b_2, and c_2 are given in Table I. Data points for $|\Delta\omega|$ in (a) were recorded at 0.05 K intervals. Only representative points are shown in the figure.

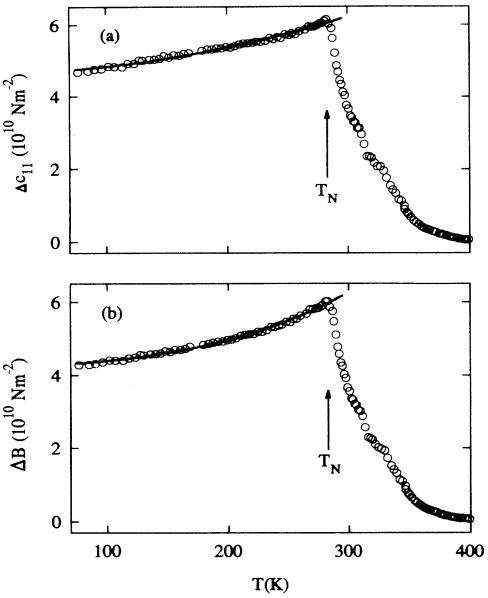

FIG. 3. The temperature dependence of the magnetic contributions (a) Δc_{11} and (b) ΔB, respectively, to c_{11} and B, of Cr–3.5 at. % Al. The solid curve in (a) is the best fit to $\Delta c_{11} = a + bt^2 + ct^4$ and that in (b) the best fit to $\Delta B = a_1 + b_1 t^2 + c_1 t^4$, where $t = T/T_N$. The fitting parameters are given in Table I.

α-T curve of Fig. 2(b). Presently there are no theoretical predictions for the exact character of the anomaly on the c-T and α-T curves of dilute Cr alloys at T_N. In previous studies[5,6] T_N was taken at the temperature of the inflection point just to the right of the minimum on the B-T or α-T curves. Usually this temperature is not too well defined. For the present crystal this temperature is about 6 K above the temperature of the minimum on the c_{11}-T, B-T, and α-T curves. The minimum and the inflection point temperatures mentioned above agree reasonably well with $T_N = 304$ K determined from the magnetic phase diagram compiled by Fawcett *et al.*[1] using all the available data on Cr-Al alloys. In this study the average temperature of the minimum on the c_{11}-T, B-T, and α-T curves, i.e., $T_N = (282 \pm 2)$ K is taken as the Néel point. This temperature is also marked on the c_{44}-T and c'-T curves of Fig. 1. Magnetic effects in the elastic constants and thermal expansion of the Cr–3.5 at. % Al crystal persist to temperatures well above T_N. This is ascribed[1] to the effects of spin fluctuations.

The magnetic contributions to the elastic constants are obtained by subtracting the measured values of the Cr–3.5 at. % Al crystal from the broken curves in Fig. 1. $\Delta B = B_{Cr_{95}V_5} - B_{Cr\text{-}Al}$ and $\Delta c_{11} = (c_{11})_{Cr_{95}V_5} - (c_{11})_{Cr\text{-}Al}$ are shown as a function of temperature in Fig. 3. The magnetic contributions to c_{11} and B are relatively large, amounting, respectively, to 19 and 44 % at T_N where they are largest. In the case of the shear constants, c_{44} and c', the magnetic contributions are relatively small, amounting, respectively, only to about 0.5 and 2 % at the lowest measured temperatures where these contributions are the largest.

The temperature dependence of ΔB, Δc_{11}, and $\Delta\omega$ below T_N were analyzed using a thermodynamic model[1] in which the magnetic free energy is given by

$$\Delta F(T,\omega) = \phi(\omega) f(t(\omega)) , \tag{1}$$

where $\phi(\omega)$ depends on the volume strain (ω) and $t(\omega) = T/T_N(\omega)$ is a reduced temperature. By assuming $f(t) = (1-t^2)^2$ and using Eq. (1), one obtains[12]

$$\Delta c_{11} = \frac{\partial^2(\Delta F)}{\partial \epsilon_{11}^2} = a + bt^2 + ct^4 , \tag{2}$$

$$\Delta B = \frac{\partial^2(\Delta F)}{\partial \omega^2} = a_1 + b_1 t^2 + c_1 t^4 , \tag{3}$$

and

$$\Delta\omega = -\frac{1}{B}\frac{\partial(\Delta F)}{\partial \omega} = a_2 + b_2 t^2 + c_2 t^4 , \tag{4}$$

where $\Delta\omega$ is the magnetovolume, ϵ is a linear strain and the b's and c's are constants containing ϕ, its first and second derivatives to strain, and T_N and the first and second derivatives of T_N to strain. As shown in Fig. 3, Eqs. (2) and (3) fit the experimental data for ΔB and Δc_{11} fairly well up to temperatures close to T_N. The fitting pa-

TABLE I. Coefficients in the expansions $\Delta c_{11}=a+bt^2+ct^4$, $\Delta B=a_1+b_1t^2+c_1t^4$, and $\Delta\omega=a_2+b_2t^2+c_2t^4$ for Cr–3.5 at. % Al.

Δc_{11}		ΔB		$\Delta\omega$	
$a(10^{10}\ \mathrm{Nm}^{-2})$	4.65±0.02	$a_1(10^{10}\ \mathrm{Nm}^{-2})$	4.24±0.02	$a_2(10^{-4})$	−7.86±0.02
$b(10^{10}\ \mathrm{K}^{-2})$	1.4±0.1	$b_1(10^{10}\ \mathrm{K}^{-2})$	1.2±0.2	$b_2(10^{-4})$	3.1±0.2
$c(10^{8}\ \mathrm{K}^{-4})$	−6±10	$c_1(10^{9}\ \mathrm{K}^{-4})$	5.3±0.7	$c_2(10^{-4})$	3.8±0.2

rameters are shown in Table I.

Similar fits were previously[6] done successfully for Cr-Al single crystals containing 1.2 at. % Al, 1.9 at. % Al, and 2.6 at. % Al. The fitting parameters in Table I for Cr–3.5 at. % Al are of the same order of magnitudes (except for c and c_1 that are two orders of magnitude smaller) as that obtained for the above three Al concentrations. The present data together with that[2,6] on crystals containing 1.2 at. % Al, 1.9 at. % Al, 2.2 at. % Al, and 2.6 at. % Al reported previously, show a peak in both the ΔB and Δc_{11} versus concentration curves at a concentration between 2 and 2.5 at. % Al, which corresponds with the concentration for which a peak was found[5] for ΔB in measurements on polycrystalline Cr-Al alloys. There does not appear to be a systematic concentration dependence of the fitting parameters b, c, b_1, and c_1 from Table I and the previous reported data on the crystals containing 1.2 at. % Al, 1.9 at. % Al, and 2.6 at. % Al.

The fit of Eq. (4) to the experimental data for $\Delta\omega$ is shown in Fig. 2(a). The fit is fairly good with the fitting parameters shown in Table I. These fitting parameters are of the same order of magnitude as those previously obtained[5] for $\Delta\omega$ on polycrystalline Cr-Al alloys containing up to 3.2 at. % Al. The value $\Delta\omega(0)=-7.86\times10^{-4}$ is however larger than the value of about -11×10^{-4} estimated from the polycrystalline measurements. We do not know the reason for this difference but it may be mentioned that the Cr–3.5 at. % Al single crystal was confirmed to be of good quality using both x-ray and electron microprobe analyses. Unfortunately $\Delta\omega$ was not reported for the Cr-Al single crystals containing 1.2, 1.9, and 2.6 at. % Al in Ref. 6 for further comparison. The long tail above T_N in Fig. 2(a) is ascribed to the effects of spin fluctuations.

Parameters b_1, c_1, b_2, and c_2 contain[12] $\phi,\phi'=d\phi/d\omega$, $\phi''=d^2\phi/d\omega^2$, and $d\ln T_N/d\omega$ and their experimental values can be used to determine $d\ln\phi/d\omega=\phi'/\phi$ and $d\ln T_N/d\omega$. By using methods previously[12] described, one obtains for the Cr–3.5 at. % Al crystal: $d\ln T_N/d\omega=(147\pm7)$ and $d\ln\phi/d\omega=(460\pm70)$. As shown in Fig. 4, these values compare very well with values previously[6] obtained for Cr-Al crystals containing up to 2.6 at. % Al and indicate, together with the previous[6] single-crystal measurements, the presence of very large peaks in the concentration dependence of $d\ln T_N/d\omega$ and $d\ln\phi/d\omega$ at a concentration between 2 and 2.5 at. % Al.

According to the thermodynamic model[12] $(b_2/a_2+c_2/a_2)=-1$. From Table I we have $(b_2/a_2+c_2/a_2)=-0.878$, which is in reasonable agreement with the value of -1 if the approximations of the thermodynamic model are kept in mind.

The following two magnetic Grüneisen parameters that represent the strength of the magnetoelastic coupling, are defined by Fawcett *et al.*[1] for Cr and its dilute alloys,

$$\Gamma_{\mathrm{AF}}=-\frac{d\ln T_N}{d\omega}=-\frac{1}{B_N T_N}\lim_{t\to1}\left[\frac{\Delta B(t)}{\Delta\beta(t)}\right],\quad t<1\ , \tag{5}$$

$$\Gamma_{\mathrm{sf}}=-\frac{d\ln T_{\mathrm{sf}}}{d\omega}=-\frac{1}{B_N T_N}\lim_{t\to1}\left[\frac{\Delta B(t)}{\Delta\beta(t)}\right],\quad t>1\ . \tag{6}$$

The term T_{sf} is a spin-fluctuation temperature, $\Delta\beta=3\Delta\alpha$ is the magnetic contribution to the coefficient of volume thermal expansion, the suffixes AF and sf refer to the antiferromagnetic ($t<1$) and the paramagnetic ($t>1$) phases, respectively.

The requirement that Γ_{AF} and Γ_{sf} be determined only in the limit $T\to T_N$ is not stringent.[1] Plots of $\Delta B(t)$ against $\Delta\beta(t)$, both above and below T_N were found[1] to be linear in a relatively wide temperature range near T_N for several Cr alloys. Γ_{AF} and Γ_{sf} are then determined from these linear parts. A plot of $\Delta B(t)$ vs $\Delta\beta(t)$ for the Cr–3.5 at. % Al crystal is shown in Fig. 5. For $t<1$ the data are linear from $t=0.27$ to $t=0.96$ giving $\Gamma_{\mathrm{AF}}=-(140\pm6)$. The magnitude of Γ_{AF} is larger than the nearly constant value $|\Gamma_{\mathrm{AF}}|\approx90$ obtained[13] for polycrystalline Cr-Al alloys containing less than 3.2 at. % Al, showing a larger volume dependence of the magnetic ordering in single crystalline Cr–3.5 at. % Al than in the previously studied polycrystalline material. For $t>1$ the data for the Cr–3.5 at. % Al crystal do not show a useful linear region from which a value for Γ_{sf} could be obtained. This is in contrast to the behavior found in poly-

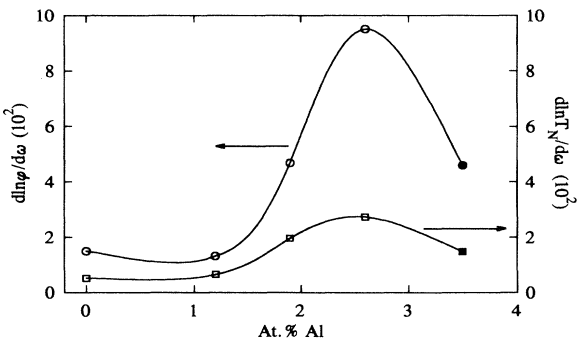

FIG. 4. The concentration dependence of $d\ln\phi/d\omega$ and $d\ln T_N/d\omega$, calculated from the thermodynamic model, for Cr-Al alloy single crystals. Points marked ○ and □ are from Ref. 6 and the points ● and ■ are from this study. The smooth curves through the points are guides to the eye.

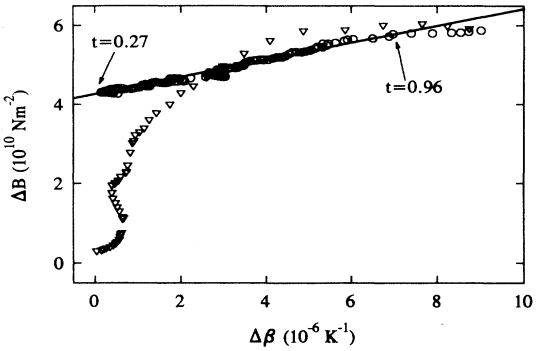

FIG. 5. Graph of the magnetic contribution to the bulk modulus $\Delta B(t)$ as a function of the magnetic contribution to the volume thermal-expansion coefficient $\Delta\beta(t)$, where $t=T/T_N$. Points marked ○ are for $T<T_N$ and those marked ▽ are for $T>T_N$. The solid line is a straight line fit to the data points between $t=0.27$ and $t=0.96$.

crystalline Cr-Al for which a useful linear region for $t>1$ was found[13] for determining Γ_{sf}.

IV. HYDROSTATIC PRESSURE DERIVATIVES OF THE SECOND-ORDER ELASTIC CONSTANTS

The pressure derivatives of the second-order adiabatic elastic constants c_{ij} were determined from the pulse-echo overlap measurements for each propagation mode as a function of pressure by using an equation given by Thurston.[14] This equation at each fixed temperature is given by

$$\left[\frac{\partial c_{ij}}{\partial P}\right]_{P=0}=(c_{ij})_{P=0}\left[2\frac{\partial f/\partial P}{f}+\frac{1}{3B}\right]_{P=0}, \quad (7)$$

where $f(P)$ is the frequency of roundtrips for the ultrasonic waves.

It is usual[14] to write Eq. (7) in terms of the natural velocity W defined as the path length at zero pressure divided by the transit time at pressure P. In terms of W Eq. (7) becomes

$$\left[\frac{\partial c_{ij}}{\partial P}\right]_{P=0}=\left[\frac{d(\rho_0 W^2)}{dP}+\frac{c_{ij}}{3B}\right]_{P=0}, \quad (8)$$

where ρ_0 is the density of the crystal at $P=0$.

Longitudinal-wave velocity measurements along [100] and [110] of the Cr–3.5 at. % Al crystal through the Néel temperature show much larger ultrasonic attenuation near T_N for [100] propagation than for [110] propagation. A large attenuation peak at T_N for longitudinal-wave propagation in Cr and its dilute alloys is a usual character and we have previously also observed larger attenuation along [100] than along [110] in other Cr alloys. However, in the case of the Cr–3.5 at. % Al crystal the attenuation along [100] near T_N is of such a magnitude that the ultrasonic signal is lost in the transition region. This is not the case for [110] longitudinal-wave propagation or for [110] and [100] shear-wave propagations. In the case of shear-wave propagation the attenuation does not change markedly in going through the Néel temperature. As applied pressure in the temperature range of this study drives the crystal through the Néel temperature, we were obliged to determine $(dc_{ij}/dP)_{P=0}$ from wave propagations along [110] only. Shear-wave propagation as a function of pressure along both [110] and [100] was used to make consistency checks for $(dc_{44}/dP)_{P=0}$, which was within the experimental error. Furthermore, [110] and [100] measurements at room temperature and atmospheric pressure served as good consistency checks for c_{44} and c_{11}.

The pressure dependence of the relative change in natural velocity $\Delta W/W_0$ for the c_L, c', and c_{44} modes is shown, respectively, in Figs. 6, 7, and 8. Here $\Delta W/W_0=(W_P/W_0)-1$, where W_0 is the natural velocity at $P=0$ and W_P that at pressure P. Values of $(dc_{ij}/dP)_{P=0}$ calculated from these curves are shown in Table II for different constant temperatures. The temperature dependence of dc_L/dP, dc_{11}/dP, dB/dP, dc_{44}/dP, and dc'/dP are shown in Fig. 9.

An interesting feature of the results in Figs. 6, 7, and 8 is the anomalous behavior observed for the pressure dependence of $\Delta W/W_0$ for all elastic modes shown. This anomalous behavior is most striking for the c_L mode. For this mode the pressure behavior of $\Delta W/W_0$ is different for temperatures below and above T_N. Well above T_N, at 373.7 K, $\Delta W/W_0$ increases linearly with applied pressure up to the highest pressures used. At 296.4 and 333.2 K $\Delta W/W_0$ for the c_L mode also in-

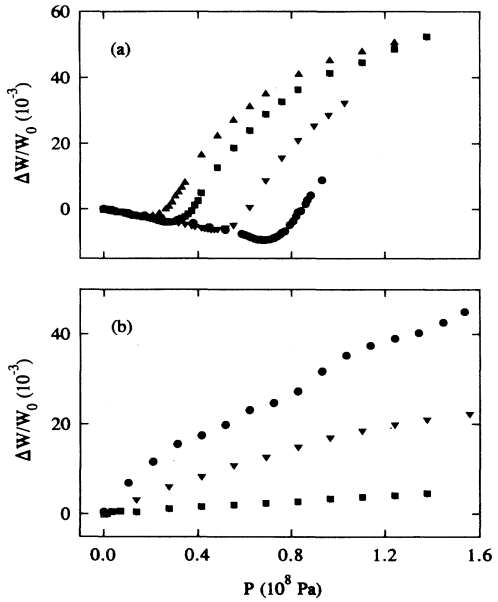

FIG. 6. Pressure dependence of the relative change in natural velocity $\Delta W/W_0$ for the c_L mode of Cr–3.5 at. % Al at (a) $T<T_N$ and (b) $T>T_N$. In (a) the points are marked as follows: $T=257$ K: ●, $T=265.1$ K: ▼, $T=273.8$ K: ■, $T=277$ K: ▲ and in (b): $T=296.4$ K: ●, $T=333.2$ K: ▼ and $T=373.7$ K: ■.

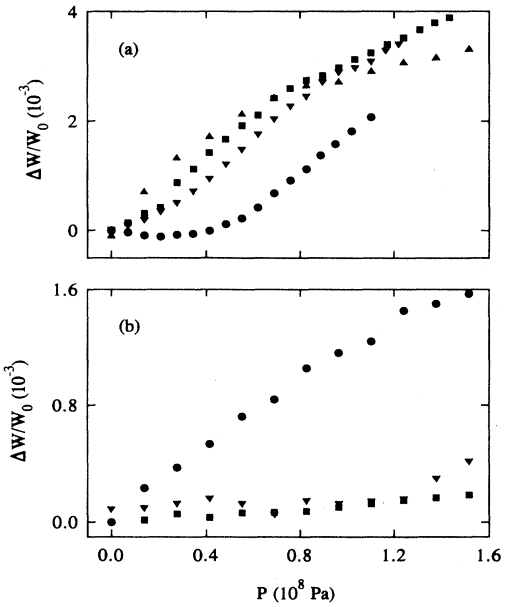

FIG. 7. Pressure dependence of the relative change in natural velocity $\Delta W/W_0$ for the c' mode of Cr–3.5 at. % Al at (a) $T < T_N$ and (b) $T > T_N$. In (a) the points are marked as follows: $T = 245.8$ K: ●, $T = 257.2$ K: ▼, $T = 265.2$ K: ■, $T = 273.6$ K: ▲ and in (b): $T = 294.6$ K: ●, $T = 328.3$ K: ▼ and $T = 372.6$ K: ■.

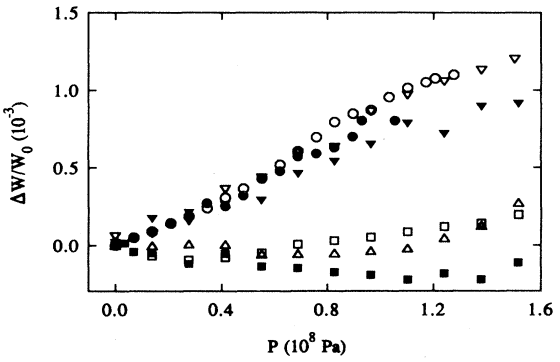

FIG. 8. Pressure dependence of the relative change in natural velocity $\Delta W/W_0$ for the c_{44} mode of Cr–3.5 at. % Al. The points are marked as follows: $T = 257.1$ K: ○, $T = 265$ K: ●, $T = 273.7$ K: ▽, $T = 291.2$ K: ▼, $T = 332$ K: □, $T = 343.5$ K: ■ and $T = 374$ K: △. It is interesting to note that the data for $T > T_N = 282$ K and that for $T < T_N$ are clustered together separately.

creases with applied pressure but this increase is nonlinear in the pressure range of the study. The behavior of the c_L mode below T_N in Fig. 6 is quite different than that for $T > T_N$. When $T < T_N = 282$ K, $\Delta W/W_0$ at first decreases linearly with increasing pressure after which it starts to increase very sharply and nonlinearly with a further increase of the pressure. The minimum in the $\Delta W/W_0$-P curves of Fig. 6 is associated with the fact that pressure at each constant temperature $T < T_N$ drives the crystal through the Néel transition to the paramagnetic phase. This moves the c_L-T curve of Fig. 1 to lower temperatures, resulting in the observed minima in the $\Delta W/W_0$-P curves of Fig. 6. These minima were used in a preliminary report[15] on the Cr–3.5 at. % Al crystal to obtain $dT_N/dP = -(370 \pm 10)$ K(GPa)$^{-1}$. The initial anomalous longitudinal-mode softening is restricted to the antiferromagnetic phase, while the behavior well above T_N, in the paramagnetic phase, is the usual linear increase in mode velocity with pressure that is normally expected for materials. No hysteresis effects were observed during increasing and decreasing pressure runs. Longitudinal-mode softening was previously[3] also observed in a Cr–0.3 at. % Ru crystal, around the ISDW-CSDW phase transition, as well as in invar iron alloys around T_N.[16]

Anomalous behavior was also observed for shear-mode propagation, but the changes in natural velocity with pressure for these modes at a constant temperature are much smaller than that observed for the longitudinal modes. In the case of the c' mode, $\Delta W/W_0$-P behaves normal at $T = 372.6$ K, which is deep enough into the paramagnetic phase, while its behavior becomes more and more anomalous (Fig. 7), as the temperature is decreased below T_N. In fact, at the lowest temperature studied for this mode, $T = 245.8$ K, the initial slope of the $\Delta W/W_0$-P curve becomes negative, showing shear-mode softening with increasing pressure at this temperature. The anomalous behavior of $\Delta W/W_0$-P for the c'

TABLE II. Elastic constants $c_L = \frac{1}{2}(c_{11} + c_{12} + 2c_{44})$, c_{44}, $c' = \frac{1}{2}(c_{11} - c_{12})$, c_{11}, c_{12}, bulk modulus B of Cr–3.5 at. % Al and their pressure derivatives at different constant temperatures through the Néel temperature, $T_N = 282$ K.

	Elastic constants (10^{11} Nm^{-2})						Pressure derivatives					
T (K)	c_L	c_{44}	c'	c_{11}	c_{12}	B	$\partial c_L/\partial P$	$\partial c_{44}/\partial P$	$\partial c'/\partial P$	$\partial c_{11}/\partial P$	$\partial c_{12}/\partial P$	$\partial B/\partial P$
257.0	2.926	1.047	1.346	3.225	0.53	1.43	−75.4	+1.3	+3.7	−73.0	−80.4	−78.0
265.1	2.910	1.046	1.346	3.210	0.52	1.42	−85.2	+1.9	+5.9	−81.2	−92.9	−89.0
273.8	2.893	1.045	1.345	3.193	0.50	1.40	−90.0	+2.0	+15.1	−76.9	−107.1	−97.0
277.0	2.887	1.044	1.344	3.186	0.50	1.39	−97.2	+2.2	+17.6	−81.8	−117.0	−105.2
296.4	3.069	1.043	1.340	3.366	0.69	1.58	+403.7	+1.6	+3.3	+405.4	+398.7	+401.0
333.2	3.298	1.042	1.333	3.589	0.92	1.81	+143.5	+0.4	+0.7	+143.9	+142.5	+143.0
373.7	3.421	1.038	1.322	3.705	1.06	1.94	+22.6	−0.3	+0.6	+23.5	+22.4	+22.7

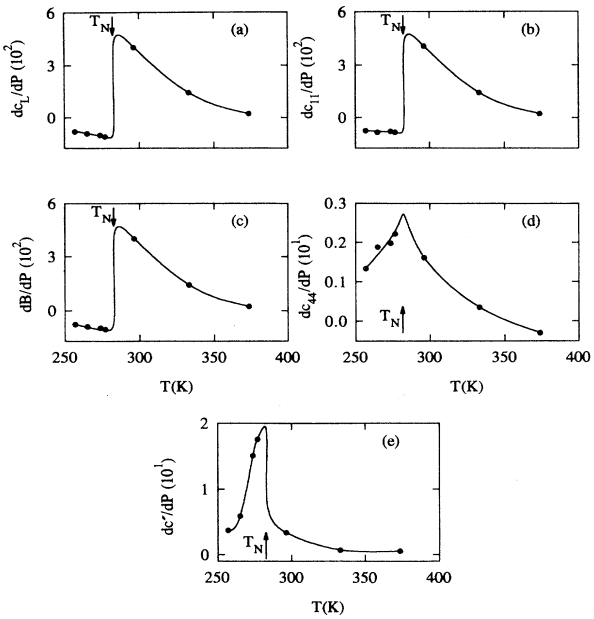

FIG. 9. The temperature dependences of (a) dc_L/dP, (b) dc_{11}/dP, (c) dB/dP, (d) dc_{44}/dP, and (e) dc'/dP for Cr–3.5 at. % Al. The smooth curves through the data points are guides to the eye.

mode must be related to the small hump in the c'-T curve (Fig. 1) observed just below T_N. When pressure is applied T_N decreases and the hump in the c'-T curve is moved to lower temperatures. Applied pressure, at constant temperatures below or near the temperature of the hump, may result in the change in initial slope of the $\Delta W/W_0$-P curves as observed in Fig. 7.

Anomalous effects in the $\Delta W/W_0$-P curves for the c_{44} mode are much smaller than that observed for the c_L and c' modes (Fig. 8). For the c_{44} mode $\Delta W/W_0$ increases with increasing P at all temperatures except for $T=343.5$ and 374 K in which cases $\Delta W/W_0$ shows an initial small decrease with increasing pressure after which it increases again. This behavior in itself is anomalous as one would expect normal behavior at least at 374 K where the c_L mode as well as the c' mode show normal behavior. The anomalous behavior of $\Delta W/W_0$ for the c_{44} mode is presently not understood.

Figure 9 shows the temperature dependences of $(dc_L/dP)_{P=0}$, $(dc_{11}/dP)_{P=0}$, $(dB/dP)_{P=0}$, $(dc_{44}/dP)_{P=0}$, and $(dc'/dP)_{P=0}$. The outstanding feature of these curves is the near discontinuous sharp increase from negative to positive values observed for $(dc_L/dP)_{P=0}$, $(dc_{11}/dP)_{P=0}$, and $(dB/dP)_{P=0}$ near T_N as well as the peaks in $(dc_{44}/dP)_{P=0}$ and $(dc'/dP)_{P=0}$ near this temperature.

The values of $|dc_L/dP|$, $|dc_{11}/dP|$, and $|dB/dP|$ associated with the longitudinal-phonon modes are much larger in the SDW phase below T_N than in the paramagnetic phase far above T_N (Fig. 9). Part of this difference in behavior may be explained in terms of the volume increase that occurs[1] when SDW antiferromagnets like Cr and its dilute alloys are cooled through T_N, i.e., the volume in the antiferromagnetic SDW phase is larger than in the paramagnetic phase as is depicted by the negative magnetovolume of Fig. 2. As the volume in the SDW state is larger than that in the paramagnetic state, one would expect the former state to be more sensitive to the effects of applied pressure than the latter. The large negative dc_{11}/dP and dB/dP in the SDW state are due to the large magnetoelastic interactions in the crystal and implies that the material becomes "softer" the more it is pressurized.

By considering Figs. 1 and 9 one concludes that magnetoelastic coupling effects are significantly larger for the volume-dependent longitudinal modes than for the volume-conserving shear modes of the Cr–3.5 at. % Al crystal.

V. GRÜNEISEN PARAMETERS OF THE Cr–3.5 at. % Al ALLOY SINGLE CRYSTAL

The Grüneisen parameter describes the anharmonic properties of a material which are responsible for the pressure dependence of the second-order elastic constants and for thermal expansion. The volume dependence of the long-wavelength acoustic-mode frequency ω_p is expressed by a mode Grüneisen parameter defined by

$$\gamma_p=-\left[\frac{\partial \ln\omega_p}{\partial \ln V}\right]_T . \tag{9}$$

γ_p is obtained from the measurements of the elastic constants and their pressure dependences using equations given by Brugger and Fritz[17] for the anisotropic continuum model. For the phonon branch p of a cubic crystal these equations are

$$\gamma(p,\mathbf{N})=-\frac{1}{6w}[3B+2w+k] , \tag{10}$$

where

$$\omega(p,\mathbf{N})=c_{11}k_1+c_{44}k_2+c_{12}k_3 ,$$

$$k(p,\mathbf{N})=c_1k_1+c_2k_2+c_3k_3 ,$$

with

$$k_1(p,\mathbf{N})=N_1^2U_1^2+N_2^2U_2^2+N_3^2U_3^2 ,$$

$$k_2(p,\mathbf{N})=(N_2U_3+N_3U_2)^2+(N_3U_1+N_1U_3)^2+(N_1U_2+N_2U_1)^2 ,$$

$$k_3(p,\mathbf{N})=2(N_2N_3U_2U_3+N_3N_1U_3U_1+N_1N_2U_1U_2) ,$$

and

$$c_1=-\left[c_{11}+3B+3B\left[\frac{\partial c_{11}}{\partial P}\right]_{P=0}\right] ,$$

$$c_2=-\left[c_{44}+3B+3B\left[\frac{\partial c_{44}}{\partial P}\right]_{P=0}\right] ,$$

$$c_3=-\left[c_{12}-3B+3B\left[\frac{\partial c_{12}}{\partial P}\right]_{P=0}\right] .$$

In these equations N_i and U_i $(i=1,2,3)$ are, respectively, the direction cosines of the wave propagation and particle displacement directions for each mode p. For a given direction of wave propagation, i.e., given N_i, the direction cosines U_i of the particle displacement directions can be obtained by solving Christoffel's equation[18]

$$(\rho v^2 \delta_{im} - c_{iklm} N_k N_j) U_m = 0 \ . \tag{11}$$

In this equation ρ is the density δ_{im} is a unit tensor, v the wave velocity, and c_{iklm} is the elastic constant tensor. Equation (11) represents a set of three homogeneous equations of the first degree with U_1, U_2, and U_3 as the unknowns. The nonzero solutions of Eq. (11) give three wave velocities, one longitudinal and two shear waves, and each wave velocity gives a different set of N_i.

A measure of the contribution of the acoustic modes at the Brillouin-zone center to the anharmonicity is given by the mean long-wavelength acoustic-mode Grüneisen parameter

$$\bar{\gamma}^{\rm el} = \frac{\sum_{p=1}^{3} \int_{\Omega} \gamma_p d\Omega}{3 \int_{\Omega} d\Omega} \ , \tag{12}$$

where the integration in Eq. (12) is over the whole of space Ω, and the γ_p's are given by Eq. (10).

The measurements for the Cr–3.5 at. % Al crystal were used to calculate γ_p as a function of mode propagation direction at each constant temperature of Table II, by using Eqs. (10) and (11). The calculations were made for propagation directions in the symmetry planes normal to the twofold and fourfold directions, as is usually done for cubic crystals.[3] Figures 10(a), 10(b), and 10(c) show the behavior of γ_p for the three modes at three representative constant temperatures of 257, 296.4, and 373.7 K. Of these three temperatures, the first is well below T_N, the second is just above T_N and the third is well above T_N, well into the paramagnetic phase.

The main feature of γ_p in Fig. 10 is the relatively large negative longitudinal-mode γ_p values in the antiferromagnetic phase at 257 K, which switch over to extremely large positive values at a temperature ($T=296.4$ K) just above T_N and then become relatively small positive in the paramagnetic phase at 373.7 K. This temperature behavior is clearly illustrated in Fig. 11 where the temperature dependence of γ_p for all three modes is shown for mode propagations along [100], [110], and [111]. The negative longitudinal-mode γ_p in the antiferromagnetic phase implies that the mode frequency and mode energy decrease with applied pressure at $T<T_N$, while the positive γ_p for this mode in the paramagnetic phase implies normal behavior, i.e., an increase in the mode frequency and energy with applied pressure.

The value and variation with wave propagation direction of γ_p for the shear modes in the CSDW phase at 257 K (Fig. 10) are roughly similar to that observed[3] for the CSDW phase of a Cr–0.3 at. % Ru crystal. These shear mode γ_p's are much smaller (Fig. 11) than the absolute value of γ_p for the longitudinal mode, similar to the observations[3] in Cr–0.3 at. % Ru. The dependence of the

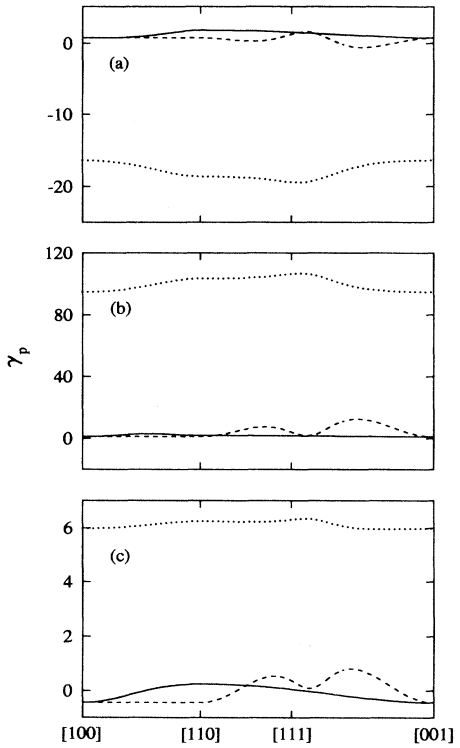

FIG. 10. Long-wavelength acoustic-mode Grüneisen parameters γ_p for Cr–3.5 at. % Al as a function of mode propagation direction at (a) $T=257$ K, (b) $T=296.4$ K, and (c) $T=373.7$ K. The longitudinal-acoustic mode γ_p is represented in (a), (b), and (c) by the dotted curve, while the solid and broken curves represent the shear acoustic-mode γ_p's in all three cases.

longitudinal mode γ_p on wave propagation direction at 257 K in the CSDW phase (Fig. 10), furthermore follows a similar pattern as was observed[3] in both the CSDW and ISDW phases of Cr–0.3 at. % Ru. This mode γ_p is negative and of approximately the same magnitude in the CSDW phases of both Cr–3.5 at. % Al and Cr–0.3 at. % Ru. In the former crystal the longitudinal mode γ_p however remains roughly constant with temperature (Fig. 11) in the CSDW phase for $T<T_N$, while its magnitude increases[3] substantially between 250 and 300 K in the CSDW phase of the latter. Figure 11(a) shows that the degenerate shear mode γ_p remains nearly temperature independent through T_N for [100] propagation. For [110] propagation the one shear mode γ_p remains constant while the other shows a relatively small effect, compared to the longitudinal γ_p, when the temperature is increased through T_N [Fig. 11(b)]. In the case of [111] propagation [Fig. 11(c)], both shear mode γ_p's show a small effect in passing through T_N. Figures 10 and 11 clearly illustrate the dominant role of the interaction between the SDW and the long-wavelength longitudinal-acoustic phonons in the behavior of the elasticity of Cr–3.5 at. % Al through the Néel transition. Shear-mode effects are relatively weak. This in a sense justifies the use of the thermodynamic models, Eqs. (1)–(4), to analyze the data for

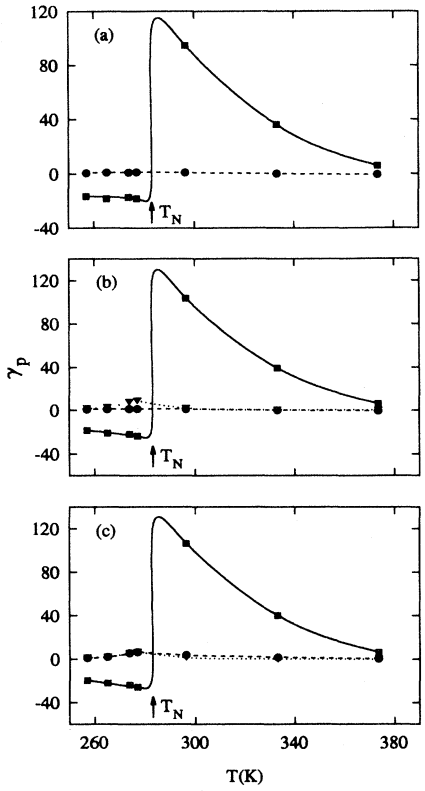

FIG. 11. Long-wavelength acoustic-mode Grüneisen parameters γ_p for Cr–3.5 at. % Al as a function of temperature for mode propagations along (a) [100], (b) [110], and (c) [111]. The longitudinal mode γ_p is represented in (a), (b), and (c) by ■, and the shear mode γ_p's by ●, and ▼ in all three cases. The curves through the data points are guides to the eye.

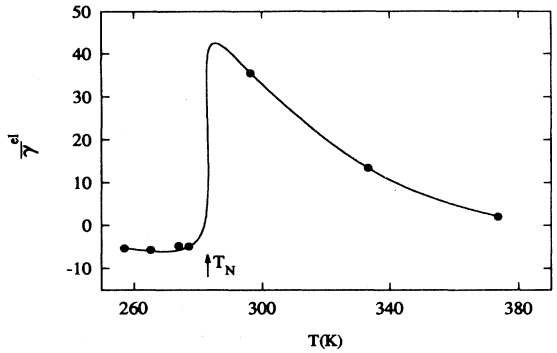

FIG. 12. The temperature dependence of the mean acoustic-mode Grüneisen parameter $\bar{\gamma}^{el}$. The curve through the data points is a guide to the eye.

the magnetoelasticity of the Cr–3.5 at. % Al crystal, as one of the assumptions of the model is that volume strain effects dominant shear effects in the magnetic free energy.

$\bar{\gamma}^{el}$ of Eq. (12) is shown as a function of temperature in Fig. 12. It is negative and nearly constant in the CSDW phase at $T < T_N$, jumps to a relatively large positive value close to T_N and then decreases towards a relatively small positive value in the paramagnetic phase. The value of $\bar{\gamma}^{el}$ is of the same order of magnitude in the CSDW phases of both Cr–3.5 at. % Al and Cr–0.3 at. % Ru, the only difference is that it remains nearly temperature independent for the former crystal while its magnitude increases with temperature for the latter.[3] The large peak in $\bar{\gamma}^{el}$ close to T_N (Fig. 12) indicates large mean vibrational anharmonicity of long-wavelength acoustic phonons near the Néel transition of Cr–3.5 at. % Al. The magnetoelastic interactions lead to the longitudinal softening (Fig. 12) in the CSDW phase. As the temperature is increased towards T_N the magnetoelastic interaction diminishes and above T_N the usual positive contribution from vibrational anharmonicity becomes dominant, giving positive $\bar{\gamma}^{el}$. A similar explanation was given[19] for the change in sign of $\bar{\gamma}^{el}$ observed in invar alloys through T_N. The unusually large positive $\bar{\gamma}^{el}$ just above T_N that decreases with increasing temperature as T goes deeper into the paramagnetic phase, may be attributed to coupling of the longitudinal phonons to the spin fluctuations as was also observed in the case[20] of invar alloys.

Reservations about the fundamental significance of magnetic Grüneisen parameters as given by Eqs. (5) and (6) were raised by Cankurtaran *et al.*[3] The main problem lies with the fact that these equations are based on the assumption that the magnetic free energy is separable from the lattice contribution in the total free energy. In practice this is not always possible.[3] It may however be instructive to note that the mean acoustic-mode Grüneisen parameter $\bar{\gamma}^{el} \approx -5$ of Cr–3.5 at. % Al is much larger in the CSDW phase than the value $\Gamma_{AF} \approx -140$ obtained from Eq. (5) for the same phase.

In conclusion, high-pressure elastic constant measurements have been used to determine the role of magnetoelastic effects in the acoustic-mode vibrational anharmonicity of Cr–3.5 at. % Al near the Néel transition. Longitudinal-mode anharmonicity plays a dominant role. The acoustic-mode Grüneisen parameter for this mode is relatively large and negative in the CSDW phase of this alloy and increases sharply to a very large positive value when the temperature is increased through the Néel point. The shear mode Grüneisen parameters are much smaller than that for the longitudinal mode, it does not change sign at the Néel transition but remains positive just below and just above T_N. The shear-mode anharmonicity is only weakly affected by the Néel transition, but its temperature dependence contributes to keep the mean long-wavelength acoustic Grüneisen parameter temperature independent in the CSDW phase just below T_N.

ACKNOWLEDGMENT

We are grateful to the South African FRD for financial support.

[1]E. Fawcett, H. L. Alberts, V. Yu. Galkin, and D. R. Noakes, Rev. Mod. Phys. **66**, 25 (1994).
[2]H. L. Alberts and P. Smit, J. Phys. Condens. Matter **6**, 3661 (1994).
[3]M. Cankurtaran, G. A. Saunders, Q. Wang, P. J. Ford, and H. L. Alberts, Phys. Rev. B **46**, 14 370 (1992).
[4]K. W. Katahara, M. Nimalendran, M. H. Manghnani, and E. S. Fisher, J. Phys. F **9**, 2167 (1979).
[5]H. L. Alberts and J. A. J. Lourens, Phys. Rev. B **29**, 5279 (1984).
[6]A. Baran, H. L. Alberts, A. M. Strydom, and P. de V. du Plessis, Phys. Rev. B **45**, 10 473 (1992).
[7]M. Bohlmann and H. L. Alberts, J. Phys. E **3**, 779 (1970).
[8]E. P. Papadakis, in *Physical Acoustics,* edited by W. P. Mason and R. N. Thurston (Academic, New York, 1976), Vol. XII.
[9]E. Kittinger, Ultrasonics **15**, 30 (1977).
[10]H. L. Alberts, J. Phys. Condens. Matter **2**, 9707 (1990).
[11]R. B. Roberts, G. K. White, and E. Fawcett, Physica **119B**, 63 (1983); and (private communication).
[12]H. L. Alberts and J. A. J. Lourens, J. Phys. Condens. Matter **4**, 3835 (1992).
[13]E. Fawcett and H. L. Alberts, J. Phys. Condens. Matter **2**, 6251 (1990).
[14]R. N. Thurston, Proc. IEEE **53**, 1320 (1965).
[15]H. L. Alberts and P. Smit, J. Magn. Magn. Mater. **145**, 152 (1995). In this preliminary report the concentration of the crystal was taken as 3.0 at. % Al, obtained from the magnetic phase diagram. The electron microprobe studies in the present report, however, show that it is in fact 3.37 at. % Al, close to the nominal concentration of 3.5 at. % Al.
[16]Ll. Mañosa, G. A. Saunders, H. Rahdi, U. Kawald, J. Pelzl, and H. Bach, Phys. Rev. B **45**, 2224 (1992).
[17]K. Brugger and T. C. Fritz, Phys. Rev. **157**, 524 (1967).
[18]H. B. Huntington, *Solid State Physics: Advances in Research and Applications,* edited by F. Seitz and D. Turnbull (Academic, New York, 1958), Vol. 7.
[19]Ll. Mañosa, G. A. Saunders, H. Rahdi, U. Kawald, J. Pelzl, and H. Bach, J. Phys. Condens. Matter **3**, 2273 (1991).
[20]G. P. Renaud and S. G. Steinemann, J. Magn. Magn. Mater. **45**, 126 (1984).